ACS APPLIED BIO MATERIALS

www.acsabm.org Article

^{1}H NMR Relaxometric Study of Chitosan-Based Nanogels Containing Mono- and Bis-Hydrated Gd(III) Chelates: Clues for MRI Probes of Improved Sensitivity

Fabio Carniato, Lorenzo Tei, Mauro Botta,* Enrico Ravera, Marco Fragai, Giacomo Parigi, and Claudio Luchinat*

Cite This: *ACS Appl. Bio Mater.* 2020, 3, 9065−9072 Read Online

ACCESS | Metrics & More | Article Recommendations | Supporting Information

ABSTRACT: Hydrogel nanoparticles composed of chitosan and hyaluronate and incorporating Gd-based MRI contrast agents with different hydration number (e.g., $[Gd(DOTA)(H_2O)]^-$ and $[Gd(AAZTA)(H_2O)_2]^-$) were prepared and fully characterized. In particular, ^{1}H NMR relaxometric data, acquired as a function of temperature and applied magnetic field strength, were for the first time thoroughly analyzed using a theoretical model that includes the effects of a static zero-field splitting and an anisotropic molecular tumbling. The paramagnetic nanoparticles show excellent stability in aqueous solution for over 150 h and do not release the load of Gd(III) chelates. These nanoparticles exhibit enhanced efficacy (relaxivity) as relaxation agents, over 6 times that of the free complexes, thanks to the combination of a restricted molecular dynamics in the presence of a fast exchange of metal-bound water molecule(s) and between the water inside the nanogel and the bulk water. The knowledge of the molecular parameters that control the effectiveness of these MRI nanoprobes and those that limit their further increase will be crucial for the development of optimized systems with high sensitivity and stability.

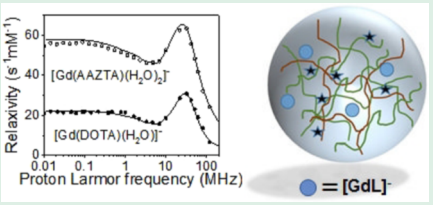

KEYWORDS: *nanogels, gadolinium (III), MRI nanoprobes, relaxometry, cyclic ligands*

INTRODUCTION

Within a few years after its discovery, magnetic resonance imaging (MRI) has developed as one of the most important imaging modalities and has established itself as a technique of great relevance in clinical diagnostic medicine, preclinical studies, and biomedical research. Essentially, the clinical utility of magnetic resonance imaging is based on the fact that the values of the longitudinal (T_1) and transverse (T_2) nuclear magnetic relaxation times of the mobile water protons of tissues vary from one tissue to another.[1] Furthermore, these parameters vary between healthy and pathological tissues. Therefore, as pointed out by S. Koenig more than three decades ago, MRI images are essentially maps of tissue-specific relaxation rates of tissue water protons and only marginally maps of proton density.[2] If there is little contrast between healthy and pathological regions resulting from the occurrence of very small differences in relaxation times, the use of a contrast agent (CA) has proven to be extremely useful for a more accurate and rapid diagnosis. In fact, the remarkable success and bursting development of MRI have been helped considerably by the chemical and magnetic properties of the contrast agents.[3−7] For the reasons mentioned above, the CAs available on the market or developed for clinical or preclinical studies are mainly represented by paramagnetic compounds capable of significantly varying the values of T_1 and T_2 of tissue water protons in the regions in which they are distributed. Predominantly, clinically used CAs are coordination complexes in which a Gd^{III} ion is encapsulated within octadentate chelators based on polyaminocarboxylate anions. The reasons for this prevalence of Gd-based CAs derive from the almost optimal magnetic properties of the Gd^{III} ion (i.e., a high magnetic moment associated with the presence of seven unpaired electrons and long electronic relaxation times) combined with the indispensable chemical characteristics of its complexes, e.g., high thermodynamic stability and good kinetic inertia, high aqueous solubility, remarkable stability of the oxidation state, and low osmolality.[1−5] Given these premises, it is not surprising that after the first human images measured in 1984 using $[GdDTPA(H_2O)]^{2-}$,[8] the use of Gd-based CAs in MRI has grown rapidly, soon becoming routine in clinical practice. Their use is mandatory in the visualization of small tumor lesions and in the assessment of functional abnormalities. As reported in a recent and excellent review on this topic, Gd-based CAs are used in about 40% of all MRI exams and in about 60% of neuro MRI exams. This

Received: October 7, 2020
Accepted: November 18, 2020
Published: December 1, 2020

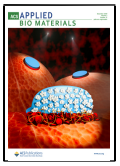

https://dx.doi.org/10.1021/acsabm.0c01295
ACS Appl. Bio Mater. 2020, 3, 9065−9072

corresponds to approximately 40 million administrations per year of Gd^{III} chelates worldwide.[3]

Despite all of these clear evidences of remarkable success, some difficult challenges remain to be addressed and overcome. The most important are related to safety and improved efficacy. In 2006 a new, very serious, even lethal pathological state, called nephrogenic systemic fibrosis (NSF), was associated with the release of Gd^{3+} ions from MRI CAs in patients with impaired renal clearance.[9−11] Much more recently, an increasing amount of data has highlighted a process of gadolinium accumulation in the tissues of patients who have received multiple administrations of Gd-based CAs. These results have attracted considerable attention and raised new concerns about the safety profile of these diagnostic probes, even if so far there are no indications of consequences on the health of patients caused by the deposition of Gd.[12,13] An approach for the design of imaging agents of enhanced safety consists in the development of systems with significantly greater efficacy (relaxivity). Simply, these high-relaxivity CAs could significantly decrease the dose needed to be administered for clinical purposes (typically, 0.1 mmol of Gd kg^{-1}). In fact, it is well known that clinically used MRI contrast agents have a value of relaxivity that is only a small fraction of the theoretically possible maximum value.[7]

The confinement of Gd(III) chelates within nanogels (NG) can be considered as a new route to hypersensitive MRI probes. In fact, besides the restriction of the local reorientation degrees of freedom related to the encapsulation of CA, the high water content and its increased viscosity when entrapped within the matrix can favor a relaxivity enhancement.

Nanogels have been proposed as versatile hydrophilic systems able to entrap many guest molecules and mainly investigated as carriers of drugs or biologically active molecules.[14−16] The physicochemical properties of these matrices (particles size, shape, charge, biocompatibility) can be effectively modulated by modifying their chemical composition and the synthetic procedures. This high versatility along with the high variability of the guest molecules that can be confined offers distinct advantages, opening the way to different nanogels with biomedical applications.[17]

Most of the nanogels described in the literature are stabilized by noncovalent interactions (ionic, H-bonds, hydrophobic forces) between biocompatible polymers such as chitosan, hyaluronic acid, or oligo/polypeptide-based systems.[17,18] It is reasonable to expect that Gd(III) chelates, when sequestered within nanosized matrices, will be unavailable to endogenous chelators or metal ions, thus avoiding transmetallation processes and eventually Gd^{3+} release.

Furthermore, it has been recently shown that some negatively charged Gd(III) complexes embedded in chitosan/hyaluronate-based nanogels experienced a 22 times relaxivity increase in the 0.5−1.4 T magnetic field range in comparison to the nonencapsulated chelates.[19−21] Nevertheless, the physical reasons for such an increase are not fully understood, being probably linked to the restriction of molecular tumbling motions of the Gd(III) complex combined with the alteration of the dynamics of water molecules within the nanogel compartment.

Taking the basis from these data, we extended the study on chitosan- and hyaluronate-based NGs embedding two different Gd(III) complexes with different coordination geometries and hydration states. We considered the clinically approved monohydrated (q = 1) $[Gd(DOTA)(H_2O)]^-$ (DOTA = (1,4,7,10-tetraaza cyclododecane-1,4,7,10-tetraacetic acid))[22] and the bis-hydrated (q = 2) $[Gd(AAZTA)(H_2O)_2]^-$ (AAZTA = 6-amino-6-methylperhydro-1,4-diazepine-*N*,*N*′,*N*″,*N*‴-tetraacetic acid)[23] (Scheme 1).

Scheme 1. Schematic View of the Nanogel Matrix Functionalized with $[Gd(DOTA)(H_2O)]^-$ and $[Gd(AAZTA)(H_2O)_2]^-$ Chelates

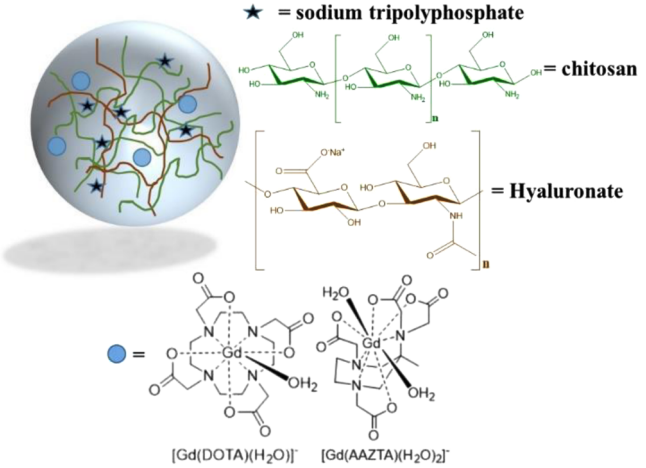

A multiparametric ^1H NMR relaxometric analysis was applied for the first time by measuring the proton longitudinal relaxation rate (R_1) as a function of the applied magnetic field (from 0.01 to 120 MHz) and temperature, with the aim of extrapolating the molecular, dynamic, and electronic parameters responsible for the increased performance of these nanosystems.

MATERIALS AND METHODS

Chemicals and Materials. All chemicals were purchased from Sigma-Aldrich Co. and used without further purification. Electrospray ionization mass spectra (ESI MS) were recorded using an SQD 3100 Mass Detector (Waters), operating in positive- or negative-ion mode, with 1% v/v formic acid in methanol as the carrier solvent.

$[Gd(AAZTA)(H_2O)_2]^-$. AAZTA (10 mg, 0.028 mmol) was dissolved in 5 mL of pure water. A slight stoichiometric excess (ca. 5%) of $GdCl_3{\cdot}6H_2O$ was added, and the solution was stirred for 2 h at room temperature, maintaining the pH around neutrality with a diluted NaOH solution (0.5 M). The pH was then increased to 9.5 to precipitate excess Gd(III) as $Gd(OH)_3$. The solution was centrifuged (4000 rpm, 3 min, rt), and the supernatant was filtered through a 0.2 μm filter. The pH was readjusted to 7, and finally, $[Gd(AAZTA)(H_2O)_2]^-$ was isolated by lyophilization. This procedure ensures the absence of excess ligand or free metal ion in the final solution. Thus, the xylenol orange test[24] verified the absence of free Gd^{3+}. MS ESI$^-$ (m/z) = 514.2 $[M]^-$; calculated $C_{14}H_{19}GdN_3O_8$ = 514.6.

$[Gd(DOTA)(H_2O)]^-$. H_4DOTA (20 mg, 0.05 mmol) was dispersed in 8 mL of pure water. A slight stoichiometric excess (ca. 5%) of $GdCl_3{\cdot}6H_2O$ was added, and the solution was stirred for 12 h at room temperature, maintaining the pH around neutrality with a diluted NaOH solution (0.5 M). The purification procedure is the same as that reported for $[Gd(AAZTA)(H_2O)_2]^-$. MS ESI$^-$ (m/z) = 558.1 $[M]^-$; calculated $C_{16}H_{27}GdN_4O_8$ = 557.6.

Nanogel Formulation (NG). The pure nanogel matrix was prepared by adapting a procedure reported in the literature.[19] In detail, 22.5 mg of chitosan (Sigma-Aldrich 740063-5G) was dissolved in 9 mL of an acetic acid solution (10 wt %). In parallel, an anionic solution was prepared, composed of 5.4 mg of sodium tripolyphosphate (TPP, Alfa Aesar 13440) and 3.6 mg of sodium hyaluronate (Hya, Alfa Aesar J66993) in 4.5 mL of pure water (Scheme S1). After

https://dx.doi.org/10.1021/acsabm.0c01295
ACS Appl. Bio Mater. 2020, 3, 9065−9072

complete solubilization of all of the products, the anionic solution was added dropwise to the chitosan solution and the reaction mixture was stirred for 30 min at room temperature, until complete formation of nanoparticles homogeneously dispersed in the matrix. The final suspension was purified by dialysis using a membrane with cutoff of 14.000 Da in pure water. To remove the excess of reactants not involved in the reaction, the procedure was carried out for 3 days with regular water replacement.

Confinement of $[Gd(DOTA)(H_2O)]^-$ and $[Gd(AAZTA)(H_2O)_2]^-$ Chelates in the Nanogel Matrix. The composite materials were prepared by ionotropic gelation following the same procedure as that reported for the synthesis of the pure nanogel (Scheme S1). In both cases, 7.7 mg of $[Gd(DOTA)(H_2O)]^-$ or $[Gd(AAZTA)(H_2O)_2]^-$ was introduced in the polyanionic solution containing TPP and Hya.

Characterization Techniques. Elemental analyses were performed on a Thermo Fisher Scientific X5 Series inductively coupled plasma-mass spectrometer (ICP-MS; Waltham, MA). Prior to the analysis, the nanogel formulations were dehydrated and the solid samples were mineralized by treatment with nitric acid at 373 K for 24 h.

The concentration of the Gd(III) chelates in the nanogel suspensions was assessed by both ICP-MS and ^{1}H NMR measurements using the bulk magnetic susceptibility (BMS) method[25,26] with a Bruker Avance III spectrometer equipped with a wide-bore 11.7 T magnet.

The water content entrapped in the nanogels was determined by gravimetric approach. A small volume of the suspension (5 mL) was centrifuged at 10 000 rpm for 1 h at 7 °C. The hydrated solid was weighed and treated at 100 °C for 24 h to remove the entrapped water.[19] The water content was calculated using eq 1

$$\text{water amount (\%)} = \frac{m_{NG}^{wet} - m_{NG}^{dried}}{m_{NG}^{wet}} \times 100 \quad (1)$$

Dynamic light scattering (DLS) and ζ-potential experiments were carried out at 298 K using a Malvern Zetasizer NanoZS operating in a particle size range of 0.6−6 mm and equipped with a He−Ne laser with λ = 633 nm.

$1/T_1$ ^{1}H nuclear magnetic relaxation dispersion (NMRD) profiles were measured on a fast-field cycling (FFC) Stelar SmarTracer Relaxometer over a continuum of magnetic field strengths from 0.00024 to 0.25 T (corresponding to 0.01−10 MHz proton Larmor Frequencies). The relaxometer operates under computer control with an absolute uncertainty in $1/T_1$ of ± 1%. Additional data in the 20−120 MHz frequency range were obtained with a High Field Relaxometer (Stelar) equipped with the HTS-110 3T Metrology cryogen-free superconducting magnet. The data were collected using the standard inversion recovery sequence (20 experiments, 2 scans) with a typical 90° pulse width of 3.5 μs, and the reproducibility of the data was within ±0.5%.

The temperature dependence of the relaxivity was analyzed at 20 MHz with the Stelar High Field Relaxometer (see above). The diamagnetic contribution was measured by collecting ^{1}H NMRD profiles of the unloaded nanoparticles, at different temperatures. The relaxivity (r_1, mM^{-1} s^{-1}) at different magnetic fields and temperatures was obtained by measuring the longitudinal relaxation rates of the paramagnetic suspensions and subtracting the diamagnetic contribution measured for the GdL-unloaded particles. The final values were divided by the mM concentration of the Gd^{3+} chelates in the suspension.

RESULTS AD DISCUSSION

The nanogel formulation utilized in this work was adapted from an optimized procedure previously reported in the literature,[19] based on an ionotropic gelation of the chitosan matrix in the presence of an anionic component composed of sodium hyaluronate and a cross-linking agent (TPP). The gelation reaction rapidly occurred in a few minutes in acidic solution at room temperature. During the particles growth, the selected Gd(III) chelates, previously dissolved in the anionic solution, were entrapped into the matrix by exploiting ionic interaction with the protonated chitosan chains. This avoids a possible release of the metal complexes during the purification steps, which were carried out through dialysis in aqueous solution. During this purification procedure, the pH of the nanogel formulation increased from 2.7 to ca. 5.0.

The amount of Gd(III) complexes used in the synthesis (ca. 0.9 mM) was chosen to ensure a high load of Gd^{3+} in the final nanoparticles. The dispersion degree and the stability of the colloidal suspensions were evaluated by DLS analysis at 298 K. The pure NG and the formulation containing $[Gd(AAZTA)(H_2O)_2]^-$ are composed of particles with a size of ca. 200 nm and a polydispersity index (PDI) of 0.54 and 0.60, respectively (Figure 1). Micrometric aggregates are also visible in both the

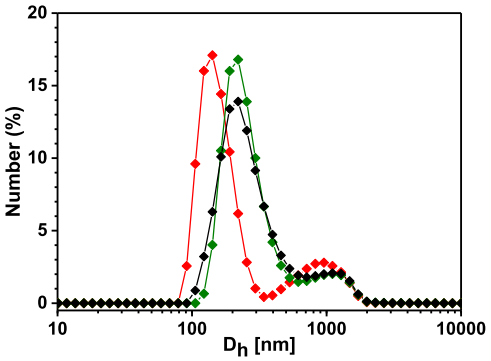

Figure 1. DLS analysis of NG (black), NG/$[Gd(DOTA)(H_2O)]^-$ (red), and NG/$[Gd(AAZTA)(H_2O)_2]^-$ (green).

suspensions. A similar behavior was observed for the NG/$[Gd(DOTA)(H_2O)]^-$ suspension, although the particles showed a maximum particles diameter distribution around 150 nm with a PDI of 0.42 (Figure 1). The high PDI values observed for the nanogels are affected by the presence of a small fraction of micrometric aggregates and are indicative of a heterogeneous particle size distribution. The particles sizes are comparable to those of previously published nanogels[19,20] and quite similar to those typical of liposomes.[27]

Data collected over time, up to 9 days, for the pure NG suspension indicated that the dispersion of particles is stable for over 1 week, without aggregation and sedimentation (Figure S1). The high stability of the suspensions can be attributed to the extremely high charge density exposed on the particles surface, determined by the ζ-potential parameter. DLS experiments carried out at room temperature and at pH 5 allowed us to calculate ζ-potential values of +32.9, +47.6, and +36.5 mV for NG, NG/$[Gd(DOTA)(H_2O)]^-$, and NG/$[Gd(AAZTA)(H_2O)_2]^-$ suspensions, respectively. The discrepancies in the ζ-potential values for the two formulations based on $[GdDOTA(H_2O)]^-$ and $[GdAAZTA(H_2O)_2]^-$ may be associated with the different chelate loading. In fact, the nanogels based on $[GdAAZTA(H_2O)_2]^-$ contain a double amount of negatively charged chelates compared to the sample loaded with $[GdDOTA(H_2O)]^-$, and therefore, they are characterized by a lower ζ-potential value. On the contrary, the ζ-potential value of the pure nanogel formulation appears lower. It is difficult to explain the reason for this result: probably, the presence of chelates during the gel synthesis influences the organization of the polymeric network as well as

https://dx.doi.org/10.1021/acsabm.0c01295
ACS Appl. Bio Mater. 2020, 3, 9065−9072

Table 1. r_1 and r_2/r_1 Ratio Values Measured at 20 and 60 MHz (298 K)

	$^{20}r_1$ (mM^{-1} s^{-1})	$^{60}r_1$ (mM^{-1} s^{-1})	r_2/r_1 (0.5 T)	r_2/r_1 (1.5 T)
NG/$[Gd(DOTA)(H_2O)]^-$	28.6	19.1	1.5	2.5
NG/$[Gd(AAZTA)(H_2O)_2]^-$	62.4	41.9	1.3	2.7

the final amount of polycationic and anionic agents entrapped in the structure.

Furthermore, the water content in all of the samples, determined by a gravimetric procedure (see the Materials and Methods section), was found to be in the 95−98% range for all of the samples, in perfect agreement with the hydrophilic nature of these polymeric matrices. The concentration of the Gd(III) chelates entrapped in the nanogel suspensions was quantified by ICP-MS elemental analysis after purification by dialysis. The Gd(III) loading was calculated to be 0.42 and 0.91% (w/w) for NG/$[Gd(DOTA)(H_2O)]^-$ and NG/$[Gd(AAZTA)(H_2O)_2]^-$, respectively, corresponding to a number of Gd(III) chelates per particle of ca. 3.0×10^4 and 8.4×10^4 (see ESI file).[20] On the other hand, the concentrations of the two suspensions containing NG/$[Gd(DOTA)(H_2O)]^-$ and NG/$[Gd(AAZTA)(H_2O)_2]^-$ were 0.05 and 0.22 mM, respectively.

The relaxometric properties of the paramagnetic NGs were analyzed as a function of the applied magnetic field strength and temperature and compared to those of the free $[Gd(DOTA)(H_2O)]^-$ and $[Gd(AAZTA)(H_2O)_2]^-$ chelates. The longitudinal (r_1) and transverse (r_2) proton relaxivities, at a given temperature and magnetic field strength, define the efficacy of a paramagnetic probe and correspond to the increase of the relaxation rates of water protons normalized to a 1 mM concentration of the paramagnetic agent. The r_1, and r_2/r_1 values at 298 K, and 20 and 60 MHz for NG/$[Gd(DOTA)(H_2O)]^-$ and NG/$[Gd(AAZTA)(H_2O)_2]^-$ are reported in Table 1.

With regard to the relaxivity of NG/$[Gd(DOTA)(H_2O)]^-$, it is worth highlighting that although the nanoparticles possess physicochemical properties very similar to those previously reported (GdDOTA⊂NPs),[20] the r_1 values calculated are very different: 72.3 $mM^{-1}s^{-1}$ for GdDOTA⊂NPs and 17.3 $mM^{-1}s^{-1}$ for the NG/$[Gd(DOTA)(H_2O)]^-$ discussed in this work, at 310 K and 60 MHz. This very large difference is likely associated with some different features of the nanoparticles (e.g., chitosan of a different FW) and probably to a different distribution of the complex in the nanogel matrix. Furthermore, the precise calculation of the relaxivity for GdDOTA⊂NPs has not been reported in sufficient detail.

For the purpose of describing their magnetic behavior, the Gd(III) chelates can be classified into three different environments: confined inside the matrix (fraction A), thus strongly interacting with the polymeric chains; weakly adsorbed on the outer surface (fraction B); or free in solution (fraction C). The observed longitudinal relaxation rate of the water protons in the suspension ($R_1^{tot} = 1/T_1$) is thus provided by the weighted sum of the relaxation rates of the three fractions (R_1^A, R_1^B, and R_1^C) plus the intrinsic diamagnetic relaxation rate of the NGs (R_1^D)

$$R_1^{tot} = R_1^A + R_1^B + R_1^C + R_1^D \quad (2)$$

In our case, fraction C (Gd(III) chelates free in solution) was completely removed during the dialysis procedure. On the other hand, there is no evidence for the presence of chelates weakly interacting with the outer surface of the nanogels through electrostatic interactions (fraction B). Indeed, following the procedure reported in the literature to determine physisorbed Gd(III) complexes attached to the external surface of NG,[19] our samples were high-speed-centrifuged (25 000 rpm, 4 °C, 1 h). The observed longitudinal relaxation rate (R_1) of the supernatant, isolated after centrifugation, at 30 MHz and 298 K corresponds to the diamagnetic contribution of water (0.4 s^{-1}) (Figure S2), thus confirming the absence of free chelates. Furthermore, to prove the absence of chelates weakly adsorbed on the NG surface, a preformed nanogel suspension was also mixed with a 10 mM $[Gd(DOTA)(H_2O)]^-$ solution for 5 h, to promote interactions between the complex and the positive charges of the nanogel surface. The sample was then purified by dialysis and characterized by ICP-MS. No trace of complex was detected in the final matrix.

Based on these results, we can conclude that in our case, the chelates interact strongly with the positive groups of chitosan, probably located mainly in the internal space of the NG, and are not removed by dialysis or centrifugation. Notably, dialysis was also carried out using a higher value of ionic strength (phosphate-buffered saline (PBS) 0.1 M) to minimize potential interaction between $[Gd(DOTA)(H_2O)]^-$ and the positively charged surface, but no difference in the r_1 values was observed. Therefore, in our case, only the R_1^A contribution adds to R_1^D in the expression of R_1^{tot}. The paramagnetic relaxivity r_1 was thus calculated by the ratio between $R_1^A - R_1^D$ and the total Gd concentration quantified by ICP-MS analysis (more details are reported in the ESI file).

A significant increase of the r_1 values at 20 MHz for both NGs formulations (6.5 times for NG/$[Gd(DOTA)(H_2O)]^-$ and 9 times for NG/$[Gd(AAZTA)(H_2O)_2]^-$) was observed if compared to the relaxivity values of the free chelates (Figure S3). Furthermore, the relaxivity values for the two nanocomposites remain constant over time for 5 days, thus indicating appreciable stability of the two suspensions (Figure 2). The r_2/r_1 ratio is around 1.5 and 2.5 at 20 and 60 MHz for both samples, respectively, thus indicating that these nanogels can be considered as positive MRI contrast agents.[3−6]

$1/T_1$ ^1H NMRD profiles were acquired from 0.01 to 120 MHz proton Larmor frequency at 283, 298, and 310 K (Figure 3). Consistently with the r_1 values at 20 and 60 MHz (Table 1), the proton relaxivity of NG/$[Gd(AAZTA)(H_2O)_2]^-$ is around twice that of NG/$[Gd(DOTA)(H_2O)]^-$ at all

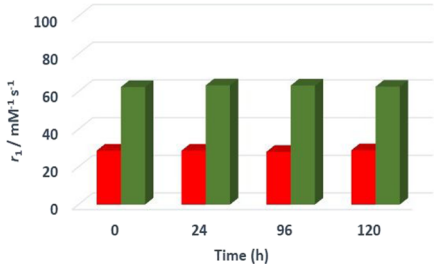

Figure 2. Time dependence of the longitudinal relaxivity for NG/$[Gd(DOTA)(H_2O)]^-$ (red) and NG/$[Gd(AAZTA)(H_2O)_2]^-$ (green) at 20 MHz and 298 K.

https://dx.doi.org/10.1021/acsabm.0c01295
ACS Appl. Bio Mater. 2020, 3, 9065−9072

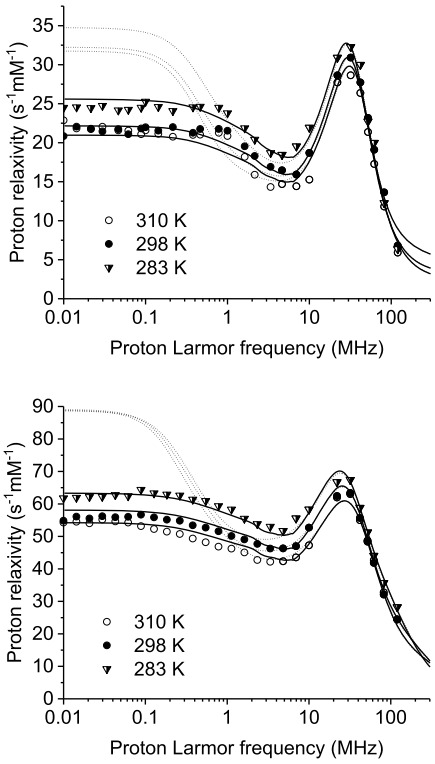

Figure 3. ^{1}H relaxivity profiles for NG/$[Gd(DOTA)(H_2O)]^-$ (up) and NG/$[Gd(AAZTA)(H_2O)_2]^-$ (down) at 283, 298, and 310 K. The solid lines indicate the best-fit profiles corresponding to the parameters reported in Tables 2 and 3; the dotted lines indicate the relaxivity profiles corresponding to the same parameters but without the static zero-field splitting (ZFS).

frequencies, as expected from the presence of two, rather than one, water molecules coordinated to the gadolinium(III) ion. This indicates that confinement in the nanoparticles does not alter the hydration state of the complex, confirming the previously observed difficulty in displacing the coordinated water molecules.[23] All profiles display a relaxivity peak at about 30 MHz, resulting from the field dependence of the correlation time modulating the gadolinium−water proton dipole−dipole interaction, and thus from a reorientation time much longer than the electron relaxation time. Since the size of the Gd chelate can only account for reorientation times smaller than 100 ps, the profiles point out that the mobility of the Gd complexes is slowed down by the strong interaction with the nanogel.

The profiles were first analyzed through the Solomon−Bloembergen−Morgan model,[28,29] but the fits are not satisfactory because of the impossibility to reproduce the positions of both the low-field and high-field dispersions with the same parameters (Figures S4 and S5). The quality of the fit does not improve with including a Lipari−Szabo order parameter[30] to consider partial averaging of the dipole−dipole interaction with local correlation times faster than the overall reorientation time. The profiles were thus fit using the modified Florence NMRD program,[31−33] which takes into account the effect of static zero-field splitting (ZFS), besides that of the transient ZFS, in determining the electron spin energy levels and the resulting transition probabilities in the coupled electron-nucleus system.[34] This allowed for a sizable increase in the quality of the fit.

The values of the best-fit parameters (reorientation time τ_R, local correlation time τ_{fast}, lifetime of coordinated water protons τ_M, correlation time for electron relaxation τ_v, transient ZFS Δ_t, squared order parameter S^2, static ZFS, and angle of the metal-nucleus vector with respect to the z-axis of the ZFS tensor) are reported in Tables 2 and 3. In the fit, the values of

Table 2. Best-Fit Parameters of the NG/$[Gd(DOTA)(H_2O)]^-$ Relaxivity Profiles[a]

	283 K	298 K	310 K	
q (*)		1		
r (*)		3.05		Å
Δ_t		0.017		cm^{-1}
τ_R	8.6	7.0	6.0	ns
τ_V	15	13	12	ps
τ_M (*)	160	135	120	ns
τ_{FAST}	160	92	63	ps
S^2		0.45		
ZFS		0.045		cm^{-1}
angle		47°		

[a]The symbol (*) indicates a fixed parameter.

Table 3. Best-Fit Parameters of the NG/$[Gd(AAZTA)(H_2O)_2]^-$ Relaxivity Profiles[a]

	283 K	298 K	310 K	
q (*)		2		
r (*)		3.05		Å
Δ_t		0.012		cm^{-1}
τ_R	9.2	6.0	4.4	ns
τ_V	12	11	10	ps
τ_M	270	220	190	ns
τ_{FAST}	1200	570	330	ps
S^2		0.49		
ZFS		0.045		cm^{-1}
angle		54°		

[a]The symbol (*) indicates a fixed parameter.

the number q of coordinated water protons and their distance r from the metal ion were fixed. Outer-sphere contributions were also included,[35] as calculated using standard values for the distance of closest approach (3.6 Å) and for the diffusion coefficients (1.5, 2.5, and 3.2 10^{-9} m^2/s at 283, 298, and 310 K, respectively). In the case of NG/$[Gd(DOTA)(H_2O)]^-$, the lifetimes were also constrained to values not shorter than those of the free $[Gd(DOTA)(H_2O)]^-$ complex in water.[36] This constraint was added because, in its absence, a fit of slightly better quality is obtained (shown in Figure S6) with lifetimes of a few nanoseconds, which seem unlikely.

The values of τ_R reach 5−10 ns (much shorter than the overall reorientation times of the 150−200 nm NG particles) with an order parameter of about 0.5. Internal correlation times τ_{fast} are about 6 times longer in NG/$[Gd(AAZTA)(H_2O)_2]^-$ than in NG/$[Gd(DOTA)(H_2O)]^-$, where it is about 90 ps at 298 K. The values of the electron relaxation parameters are in reasonably good agreement with expectations (the electron relaxation time at 298 K and low fields corresponding to 600 and 150 ps for nanogel-embedded $[Gd(DOTA)(H_2O)]^-$ and $[Gd(AAZTA)(H_2O)_2]^-$, respectively, with respect to 470[37] and 130 ps,[23] previously estimated for the free complexes), as well as the values of the static ZFS.[38−41] A smaller transient ZFS (Δ_t) for [Gd(AAZTA)-

https://dx.doi.org/10.1021/acsabm.0c01295
ACS Appl. Bio Mater. 2020, 3, 9065−9072

$(H_2O)_2]^-$ than for $[Gd(DOTA)(H_2O)]^-$ also contributes to its larger relaxivity, which is however mainly determined by the increase in the q value. The best-fit lifetime of the coordinated water protons in NG/$[Gd(AAZTA)(H_2O)_2]^-$ is somewhat longer (220 ns at 298 K) than in the free complex, where it was found to amount to 90 ns[23] at 298 K. Conversely, upon confinement into the nanogel, the fit does not reveal any increase in the lifetime of the water molecule coordinated to $[Gd(DOTA)(H_2O)]^-$ with respect to the value measured for the free complex. Although there is some covariance between this parameter and the other fit parameters so that some indetermination is possible, a slower exchange for NG/$[Gd(AAZTA)(H_2O)_2]^-$ may be related to more complex exchange schemes for this $q = 2$ complex.

The analysis of the NMRD profiles thus indicates that the confinement of the Gd complexes into the nanogel indeed increases their reorientation time to the nanoseconds time scale, likely corresponding to the correlation time for the restricted mobility of the complexes within the polymer chains network, with which they are interacting. However, the Gd complexes still retain a very fast mobility, in the hundreds of picoseconds time scale, which may be due to the different crowding of the polymer chains within the matrix. The lifetime of the water molecule(s) coordinated to the Gd ion remains short enough not to largely limit the relaxivity peak at about 0.5 T, in accordance with fast diffusion of the water molecules into the nanogel network. Furthermore, also the exchange of the water molecules embedded in the nanogel with bulk water molecules should be fast enough not to limit the relaxivity. These observations find a clear support in the dependence of relaxivity on temperature, which increases with decreasing temperature following an exponential trend, as typical of systems in the rapid exchange regime (Figure S7). Notably, sizable contributions from second-sphere water molecules are not needed for reproducing the experimental NMRD profiles, at variance with what was expected[19,20] from previously collected data.[42,43]

CONCLUSIONS

Nanogels loaded with paramagnetic metal complexes are promising systems to develop MRI probes of enhanced sensitivity. Their effectiveness as relaxation agents is at least 6 times higher than that of the free complexes in aqueous solution. The relaxivity was measured accurately as a function of temperature and applied magnetic field strength, and the data were fully analyzed, for the first time, using a model that considers the effects of a static zero-field splitting. Taking it into account allows for the analysis of the relaxation rates in the whole available frequency range and thus provides more confidence and accuracy in the values of the fit parameters. The most relevant conclusions of the study are the following: (a) the complexes show an anisotropic molecular dynamics, signaled by the considerable difference between the values of the global (τ_R) and local (τ_{fast}) reorientation correlation times; (b) the marked mobility of the embedded complexes is a feature that limits relaxivity, but that might be controlled by favoring more intense interactions with the polymer chains; and (c) the exchange of the coordinated water molecule(s) and that between the water inside the nanogel and the bulk water is fast enough not to limit relaxivity. The latter represents a key property for developing nanoprobes of improved efficacy.

In conclusion, the results of this work represent a solid base and provide useful indications for the rational design of stable, safe, and highly effective diagnostic metal-based nanoprobes. The future work will seek to further optimize the properties of the nanoparticles by appropriately varying the chemical nature of the polymer and will study the effect of the incorporation of paramagnetic complexes without coordinated water molecules ($q = 0$) on the effectiveness of the probes.

ASSOCIATED CONTENT

Supporting Information

The Supporting Information is available free of charge at https://pubs.acs.org/doi/10.1021/acsabm.0c01295.

Schematic view of the synthesis of NG incorporating Gd(III) chelates; DLS data; ^{1}H NMRD profiles of the free complexes and the final nanogels; and temperature dependence of the relaxivity for the nanogels (PDF)

AUTHOR INFORMATION

Corresponding Authors

Mauro Botta − *Dipartimento di Scienze e Innovazione Tecnologica, Università del Piemonte Orientale "Amedeo Avogadro", 15121 Alessandria, Italy;* orcid.org/0000-0003-4192-355X; Phone: +39 0131-360253; Email: mauro.botta@uniupo.it; Fax: +39 0131-360250

Claudio Luchinat − *Magnetic Resonance Center (CERM) and Department of Chemistry, University of Florence, 50019 Florence, Italy; Consorzio Interuniversitario Risonanze Magnetiche di Metalloproteine (CIRMMP), 50019 Florence, Italy;* Email: luchinat@cerm.unifi.it

Authors

Fabio Carniato − *Dipartimento di Scienze e Innovazione Tecnologica, Università del Piemonte Orientale "Amedeo Avogadro", 15121 Alessandria, Italy;* orcid.org/0000-0002-6268-1687

Lorenzo Tei − *Dipartimento di Scienze e Innovazione Tecnologica, Università del Piemonte Orientale "Amedeo Avogadro", 15121 Alessandria, Italy;* orcid.org/0000-0002-7027-8396

Enrico Ravera − *Magnetic Resonance Center (CERM) and Department of Chemistry, University of Florence, 50019 Florence, Italy; Consorzio Interuniversitario Risonanze Magnetiche di Metalloproteine (CIRMMP), 50019 Florence, Italy;* orcid.org/0000-0001-7708-9208

Marco Fragai − *Magnetic Resonance Center (CERM) and Department of Chemistry, University of Florence, 50019 Florence, Italy; Consorzio Interuniversitario Risonanze Magnetiche di Metalloproteine (CIRMMP), 50019 Florence, Italy;* orcid.org/0000-0002-8440-1690

Giacomo Parigi − *Magnetic Resonance Center (CERM) and Department of Chemistry, University of Florence, 50019 Florence, Italy; Consorzio Interuniversitario Risonanze Magnetiche di Metalloproteine (CIRMMP), 50019 Florence, Italy;* orcid.org/0000-0002-1989-4644

Complete contact information is available at: https://pubs.acs.org/10.1021/acsabm.0c01295

Author Contributions

The manuscript was written through contributions of all authors. All authors have given approval to the final version of the manuscript.

Notes

The authors declare no competing financial interest.

https://dx.doi.org/10.1021/acsabm.0c01295
ACS Appl. Bio Mater. 2020, 3, 9065−9072

■ ACKNOWLEDGMENTS

The authors acknowledge the financial support by the Ministero dell'Università e della Ricerca (PRIN 2017A2KEPL project "Rationally designed nanogels embedding paramagnetic ions as MRI probes"). F.C., L.T., and M.B. acknowledge the financial support from Università del Piemonte Orientale (Ricerca locale FAR2019). This work was carried out within the framework of the COST CA15209 Action "European Network on NMR Relaxometry".

■ REFERENCES

(1) Koenig, S. H.; Brown, R. D., III Field-cycling relaxometry of protein solutions and tissue: Implications for MRI. *Prog. Nucl. Magn. Reson. Spectrosc.* **1990**, *22*, 487−567.
(2) Koenig, S. H. Enhancement of Contrast in Magnetic Resonance Images by Paramagnetic Agents: Possibilities and Problems. *Isr. J. Chem.* **1988**, *28*, 345−353.
(3) Wahsner, J.; Gale, E. M.; Rodríguez-Rodríguez, A.; Caravan, P. Chemistry of MRI Contrast Agents: Current Challenges and New Frontiers. *Chem. Rev.* **2019**, *119*, 957−1057.
(4) Caravan, P.; Ellison, J. J.; McMurry, T. J.; Lauffer, R. B. Gadolinium(III) Chelates as MRI Contrast Agents: Structure, Dynamics, and Applications. *Chem. Rev.* **1999**, *99*, 2293−2352.
(5) Aime, S.; Botta, M.; Terreno, E. Gd(III)-based contrast agents for MRI. *Adv. Inorg. Chem.* **2005**, *57*, 173−237.
(6) Aime, S.; Geninatti Crich, S.; Gianolio, E.; Giovenzana, G. B.; Tei, L.; Terreno, E. High sensitivity lanthanide(III) based probes for MR-medical imaging. *Coord. Chem. Rev.* **2006**, *250*, 1562−1579.
(7) Helm, L.; Morrow, J. R.; Bond, C. J.; Carniato, F.; Botta, M.; Braun, M.; Baranyai, Z.; Pujales-Paradela, R.; Regueiro-Figueroa, M.; Esteban-Gomez, D.; Platas-Iglesias, C.; Scholl, T. J. Gadolinium-Based Contrast Agents. In *Contrast Agents for MRI: Experimental Methods*; The Royal Society of Chemistry, 2018. Chapter 2.
(8) Bydder, G. M.; Niendorf, H. P.; Young, I. R. Clinical Use of Intravenous Gadolinium-DTPA in Magnetic Resonance Imaging of the Central Nervous System. In *Functional Studies Using NMR*; McCready, V. R.; Leach, M.; Ell, P. J., Eds.; Springer: London, 1987.
(9) Idée, J.-M.; Port, M.; Robic, C.; Medina, C.; Sabatou, M.; Corot, C. Role of thermodynamic and kinetic parameters in gadolinium chelate stability. *J. Magn. Reson. Imaging* **2009**, *30*, 1249−1258.
(10) Di Gregorio, E.; Gianolio, E.; Stefania, R.; Barutello, G.; Digilio, G.; Aime, S. On the Fate of MRI Gd-Based Contrast Agents in Cells. Evidence for Extensive Degradation of Linear Complexes upon Endosomal Internalization. *Anal. Chem.* **2013**, *85*, 5627−5631.
(11) Marckmann, P.; Skov, L.; Rossen, K.; Dupont, A.; Damholt, M. B.; Heaf, J. G.; Thomsen, H. S. Nephrogenic Systemic Fibrosis: Suspected Causative Role of Gadodiamide Used for Contrast-Enhanced Magnetic Resonance Imaging. *J. Am. Soc. Nephrol.* **2006**, *17*, 2359−2362.
(12) Gianolio, E.; Bardini, P.; Arena, F.; Stefania, R.; Di Gregorio, E.; Iani, R.; Aime, S. Gadolinium Retention in the Rat Brain: Assessment of the Amounts of Insoluble Gadolinium-containing Species and Intact Gadolinium Complexes after Repeated Administration of Gadolinium-based Contrast Agents. *Radiology* **2017**, *285*, 839−849.
(13) McDonald, R. J.; McDonald, J. S.; Kallmes, D. F.; Jentoft, M. E.; Murray, D. L.; Thielen, K. R.; Williamson, E. E.; Eckel, L. J. Intracranial Gadolinium Deposition after Contrast-enhanced MR Imaging. *Radiology* **2015**, *275*, 772−782.
(14) Kabanov, A. V.; Vinogradov, S. V. Nanogels as pharmaceutical carriers: finite networks of infinite capabilities. *Angew. Chem., Int. Ed.* **2009**, *48*, 5418−5429.
(15) Shi, F.; Ding, J.; Xiao, C.; Zhuang, X.; He, C.; Chen, L.; Chen, X. Intracellular microenvironment responsive PEGylated polypeptide nanogels with ionizable cores for efficient doxorubicin loading and triggered release. *J. Mater. Chem.* **2012**, *22*, 14168−14179.
(16) Tang, J. D.; Mura, C.; Lampe, K. J. Stimuli-Responsive, Pentapeptide, Nanofiber Hydrogel for Tissue Engineering. *J. Am. Chem. Soc.* **2019**, *141*, 4886−4899.
(17) Wang, H.; Qian, J.; Ding, F. Recent advances in engineered chitosan-based nanogels for biomedical applications. *J. Mater. Chem. B* **2017**, *5*, 6986−7007.
(18) Neamtu, I.; Rusu, A. G.; Diaconu, A.; Nita, L. E.; Chiriac, A. P. Basic concepts and recent advances in nanogels as carriers for medical applications. *Drug Delivery* **2017**, *24*, 539−557.
(19) Callewaert, M.; Roullin, V. G.; Cadiou, C.; Millart, E.; Van Gulik, L.; Andry, M. C.; Portefaix, C.; Hoeffel, C.; Laurent, S.; Vander Elst, L.; Muller, R.; Molinari, M.; Chuburu, F. Tuning the composition of biocompatible Gd nanohydrogels to achieve hypersensitive dual T_1/T_2 MRI contrast agents. *J. Mat. Chem. B* **2014**, *2*, 6397−6405.
(20) Courant, T.; Roullin, V. G.; Cadiou, C.; Callewaert, M.; Andry, M. C.; Portefaix, C.; Hoeffel, C.; de Goltstein, M. C.; Port, M.; Laurent, S.; Vander Elst, L.; Muller, R.; Molinari, M.; Chuburu, F. Hydrogels Incorporating GdDOTA: Towards Highly Efficient Dual T_1/T_2 MRI Contrast Agents. *Angew. Chem., Int. Ed.* **2012**, *51*, 9119−9122.
(21) Rigaux, G.; Gheran, C. V.; Callewaert, M.; Cadiou, C.; Voicu, S. N.; Dinischiotu, A.; Andry, M. C.; Vander Elst, L.; Laurent, S.; Muller, R. N.; Berquand, A.; Molinari, M.; Huclier-Markai, S.; Chuburu, F. Characterization of Gd loaded chitosan-TPP nanohydrogels by a multi-technique approach combining dynamic light scattering (DLS), asymetrical flow-field-flow-fractionation (AF_4) and atomic force microscopy (AFM) and design of positive contrast agents for molecular resonance imaging (MRI). *Nanotechnology* **2016**, *28*, No. 055705.
(22) Chang, C. A.; Francesconi, L. C.; Malley, M. F.; Kumar, K.; Gougoutas, J. Z.; Tweedle, M. F.; Lee, D. W.; Wilson, L. J. Synthesis, characterization, and crystal structures of M(DO3A) (M = iron, gadolinium) and Na[M(DOTA)] (M = Fe, yttrium, Gd). *Inorg. Chem.* **1993**, *32*, 3501−3508.
(23) Aime, S.; Calabi, L.; Cavallotti, C.; Gianolio, E.; Giovenzana, G. B.; Losi, P.; Maiocchi, A.; Palmisano, G.; Sisti, M. $[Gd\text{-}AAZTA]^-$: a new structural entry for an improved generation of MRI contrast agents. *Inorg. Chem.* **2004**, *43*, 7588−7590.
(24) Barge, A.; Cravotto, G.; Gianolio, E.; Fedeli, F. How to determine free Gd and free ligand in solution of Gd chelates. A technical note. *Contrast Media Mol. Imaging* **2006**, *1*, 184−188.
(25) Evans, D. F. The determination of the paramagnetic susceptibility of substances in solution by nuclear magnetic resonance. *J. Chem. Soc.* **1959**, 2003−2005.
(26) Evans, D. F.; Fazakerley, G. V.; Phillips, R. F. Organometallic compounds of bivalent europium, ytterbium, and samarium. *J. Chem. Soc. A* **1971**, 1931−1934.
(27) Ferrauto, G.; Di Gregorio, E.; Ruzza, M.; Catanzaro, V.; Padovan, S.; Aime, S. Enzyme-Responsive LipoCEST Agents: Assessment of MMP-2 Activity by Measuring the Intra-liposomal Water ^1H NMR Shift. *Angew. Chem.* **2017**, *129*, 12338−12341.
(28) Solomon, I. Relaxation Processes in a System of Two Spins. *Phys. Rev.* **1955**, *99*, 559−565.
(29) Bloembergen, N.; Morgan, L. O. Proton Relaxation Times in Paramagnetic Solutions. Effects of Electron Spin Relaxation. *J. Chem. Phys.* **1961**, *34*, 842−850.
(30) Lipari, G.; Szabo, A. A. Model-free approach to the interpretation of nuclear magnetic resonance relaxation in macromolecules. 1. Theory and range of validity. *J. Am. Chem. Soc.* **1982**, *104*, 4546−4559.
(31) Bertini, I.; Galas, O.; Luchinat, C.; Parigi, G. A Computer Program for the Calculation of Paramagnetic Enhancements of Nuclear-Relaxation Rates in Slowly Rotating Systems. *J. Magn. Reson., Ser. A* **1995**, *113*, 151−158.
(32) Bertini, I.; Kowalewski, J.; Luchinat, C.; Nilsson, T.; Parigi, G. Nuclear spin relaxation in paramagnetic complexes of S = 1: Electron spin relaxation effects. *J. Chem. Phys.* **1999**, *111*, 5795−5807.

https://dx.doi.org/10.1021/acsabm.0c01295
ACS Appl. Bio Mater. 2020, 3, 9065−9072

(33) Kruk, D.; Nilsson, T.; Kowalewski, J. Nuclear spin relaxation in paramagnetic systems with zero-field splitting and arbitrary electron spin. *Phys. Chem. Chem. Phys.* **2001**, *3*, 4907−4917.
(34) Kowalewski, J.; Kruk, D.; Parigi, G. NMR relaxation in solution of paramagnetic complexes: recent theoretical progress for $S \geq 1$. *Adv. Inorg. Chem.* **2005**, *57*, 41−104.
(35) Freed, J. H. Dynamic effects of pair correlation functions on spin relaxation by translational diffusion in liquids. II. Finite jumps and independent T_1 processes. *J. Chem. Phys.* **1978**, *68*, 4034−4037.
(36) Laurent, S.; Vander Elst, L.; Muller, R. N. Comparative study of the physicochemical properties of six clinical low molecular weight gadolinium contrast agents. *Contrast Media Mol. Imaging* **2006**, *1*, 128−137.
(37) Powell, D. H.; Ni Dhubhghaill, O. M.; Pubanz, D.; Helm, L.; Lebedev, Y. S.; Schlaepfer, W.; Merbach, A. E. Structural and Dynamic Parameters Obtained from ^{17}O NMR, EPR, and NMRD Studies of Monomeric and Dimeric Gd^{3+} Complexes of Interest in Magnetic Resonance Imaging: An Integrated and Theoretically Self-Consistent Approach. *J. Am. Chem. Soc.* **1996**, *118*, 9333−9346.
(38) Rotz, M. W.; Culver, K. S. B.; Parigi, G.; MacRenaris, K. W.; Luchinat, C.; Odom, T. W.; Meade, T. J. High Relaxivity Gd(III)−DNA Gold Nanostars: Investigation of Shape Effects on Proton Relaxation. *ACS Nano* **2015**, *9*, 3385−3396.
(39) Li, H.; Parigi, G.; Luchinat, C.; Meade, T. J. Bimodal Fluorescence-Magnetic Resonance Contrast Agent for Apoptosis Imaging. *J. Am. Chem. Soc.* **2019**, *141*, 6224−6233.
(40) Caravan, P.; Parigi, G.; Chasse, J. M.; Cloutier, N. J.; Ellison, J. J.; Lauffer, R. B.; Luchinat, C.; McDermid, S. A.; Spiller, M.; McMurry, T. J. Albumin Binding, Relaxivity, and Water Exchange Kinetics of the Diastereoisomers of MS-325, a Gadolinium(III)-Based Magnetic Resonance Angiography Contrast Agent. *Inorg. Chem.* **2007**, *46*, 6632−6639.
(41) Mastarone, D. J.; Harrison, V. S. R.; Eckermann, A. L.; Parigi, G.; Luchinat, C.; Meade, T. J. A Modular System for the Synthesis of Multiplexed Magnetic Resonance Probes. *J. Am. Chem. Soc.* **2011**, *133*, 5329−5337.
(42) Botta, M.; Tei, L. Relaxivity Enhancement in Macromolecular and Nanosized Gd^{III}-Based MRI Contrast Agents. *Eur. J. Inorg. Chem.* **2012**, *2012*, 1945−1960.
(43) Gambino, G.; Tei, L.; Carniato, F.; Botta, M. Amphiphilic Ditopic Bis-Aqua Gd-AAZTA-like Complexes Enhance Relaxivity of Lipidic MRI Nanoprobes. *Chem. Asian J.* **2016**, *11*, 2139−2143.

https://dx.doi.org/10.1021/acsabm.0c01295
ACS Appl. Bio Mater. 2020, 3, 9065−9072